Neuron

Report

Optimized deep brain stimulation for anterior cingulate cortex inhibition produces antidepressant-like effects in mice

Graphical abstract

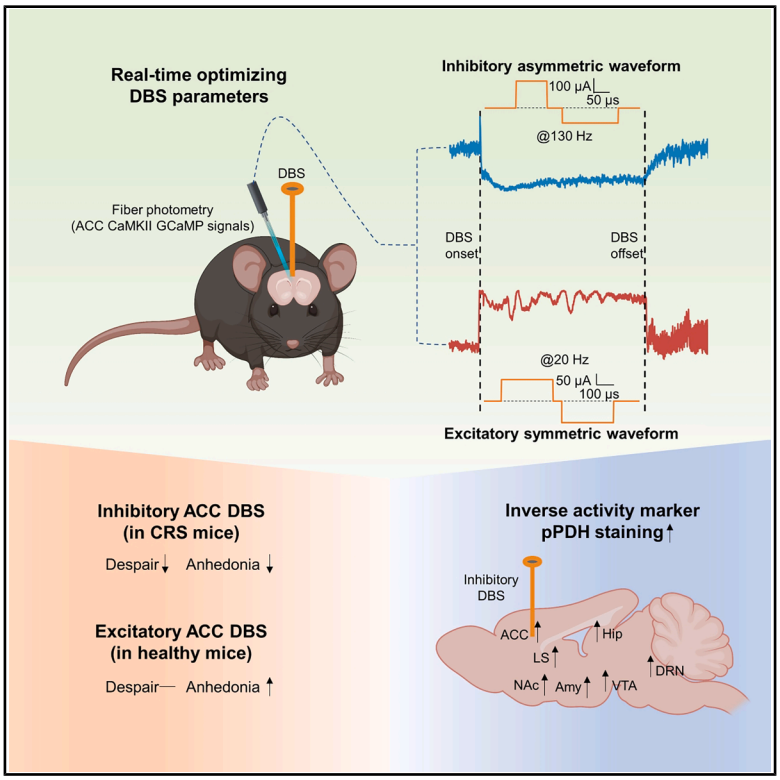

Highlights

- Optimized DBS parameters bidirectionally control ACC pyramidal neuron activity
- Inhibition of the ACC produces rapid and sustained antidepressant-like effects
- Activation of the ACC induces anhedonia-like behavior
- ACC inhibition suppresses activity in a brain-wide network for mood regulation

Authors

Zhengwei Yuan, Haonan Yang, Peng Wang, ..., Jianning Zhang, Zhiqi Mao, Minmin Luo

Correspondence

yuanzhengwei@cibr.ac.cn (Z.Y.), markmaoqi@163.com (Z.M.), luominmin@cibr.ac.cn (M.L.)

In brief

Yuan et al. combine deep brain stimulation with neural activity monitoring to optimize stimulation parameters for the anterior cingulate cortex. They show that inhibitory DBS produces rapid, long-lasting antidepressant-like effects and suppresses mood-regulating networks, offering a circuit-based blueprint for optimizing neuromodulation therapies.

Yuan et al., 2025, Neuron *113*, 1–11
October 15, 2025
https://doi.org/10.1016/j.neuron.2025.07.018

CellPress

Neuron

CellPress

Report

Optimized deep brain stimulation for anterior cingulate cortex inhibition produces antidepressant-like effects in mice

Zhengwei Yuan,[1,2,10,*] Haonan Yang,[3,10] Peng Wang,[1,2] Xiaoning Hou,[1,2] Ke Xu,[4] Yu Zhou,[1,2] Ruicheng Dai,[1,2] Yuan Gao,[1,2] Xinwei Gao,[1,2] Qingchun Guo,[1,2] Yulong Li,[6,7] Jianning Zhang,[3] Zhiqi Mao,[3,8,*] and Minmin Luo[1,2,5,6,9,11,*]

[1]Beijing Institute for Brain Research, Peking Union Medical Collage and Chinese Academy of Medical Sciences, Beijing 102206, China
[2]Chinese Institute for Brain Research, Beijing 102206, China
[3]Department of Neurosurgery, Chinese PLA General Hospital First Medical Center, Beijing 100000, China
[4]Department of Neurosurgery, SanBo Brain Hospital, Capital Medical University, Beijing 100093, China
[5]Research Unit of Medical Neurobiology, Chinese Academy of Medical Sciences, Beijing 102206, China
[6]New Cornerstone Science Laboratory, Shenzhen 518054, China
[7]School of Life Science, Peking University, Beijing 100871, China
[8]Department of Neurosurgery, Neuromedicine Center, Beijing Shijitan Hospital, Capital Medical University, Beijing 100038, China
[9]Beijing Tiantan Hospital, Beijing 100070, China
[10]These authors contributed equally
[11]Lead contact
*Correspondence: yuanzhengwei@cibr.ac.cn (Z.Y.), markmaoqi@163.com (Z.M.), luominmin@cibr.ac.cn (M.L.)
https://doi.org/10.1016/j.neuron.2025.07.018

SUMMARY

Deep brain stimulation (DBS) emerges as a promising intervention for psychiatric disorders, including major depressive disorder (MDD). The optimal stimulation parameters and the neural circuit mechanisms of DBS remain areas of active investigation. This study combines DBS with fiber photometry to monitor neuronal activity in the mouse anterior cingulate cortex (ACC), a key region implicated in depression. By systematically optimizing DBS parameters—including waveform, pulse width, and frequency—we identified configurations that robustly inhibited or activated ACC activity. Inhibitory DBS elicited rapid-onset and long-lasting antidepressant-like behaviors in mouse models of depression, while excitatory DBS induced anhedonia in otherwise healthy mice. Using an inverse activity marker, we mapped the downstream effects of ACC DBS, revealing broad inhibition across emotion- and mood-regulation networks. These findings establish a principled framework for DBS parameter optimization and identify ACC-targeted inhibition as a potential therapeutic strategy for MDD.

INTRODUCTION

Deep brain stimulation (DBS) has become a cornerstone treatment for neurological disorders such as Parkinson's disease, essential tremor, and dystonia.[1,2] Recently, DBS has also shown promise for treatment-resistant major depressive disorder (MDD), with subcallosal cingulate (SCC) stimulation achieving sustained remission in ~25% of patients.[3–5] However, outcome variability and limited mechanistic understanding hinder broader application. A critical gap remains in defining how stimulation parameters influence neural circuits to achieve therapeutic effects.

The anterior cingulate cortex (ACC) is a key region implicated in mood regulation and MDD pathophysiology. Structural, biochemical, and metabolic alterations in the ACC are consistently observed in MDD patients and animal models.[6–8] The ACC is also central to the antidepressant effects of rapid-acting treatments like ketamine.[9] Preclinical studies further link depression to ACC hyperactivity, demonstrating that chemogenetic or optogenetic inhibition of ACC neurons alleviates depressive-like behaviors.[10,11] While these approaches highlight therapeutic potential, their clinical applicability remains limited. DBS offers a precise, reversible, and clinically viable alternative for real-time ACC modulation. However, existing protocols are largely empirical and lack mechanistic grounding,[12,13] limiting optimization.

A central challenge is determining how stimulation parameters influence circuit activity. While some studies suggest DBS exerts inhibitory effects,[14] others report excitation.[15–17] These divergent findings underscore the need for real-time monitoring to resolve whether DBS inhibits or excites circuits, and under what conditions each mode is therapeutic. Seminal work established intermittent SCC local field potentials as DBS biomarkers,[18] advancing individualized therapy. In humans, however, stimulation artifacts restrict analysis to post-stimulation epochs and preclude cellular resolution. Preclinical models

Please cite this article in press as: Yuan et al., Optimized deep brain stimulation for anterior cingulate cortex inhibition produces antidepressant-like effects in mice, Neuron (2025), https://doi.org/10.1016/j.neuron.2025.07.018

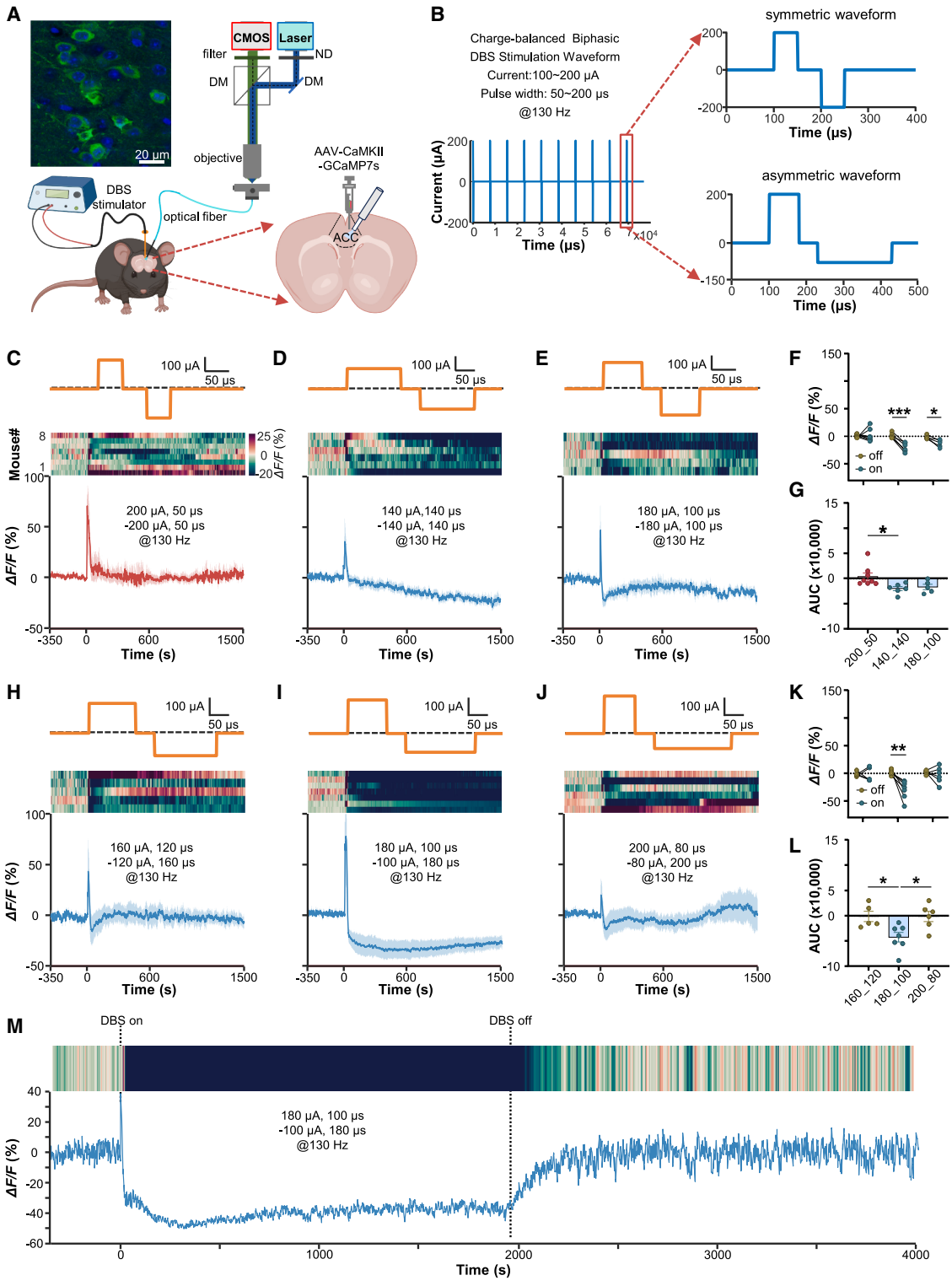

Figure 1. Optimization of DBS parameters for inhibiting ACC CaMKII⁺ neurons

(A) Schematic of simultaneous DBS and fiber photometry of Ca^{2+} signals from ACC pyramidal neurons expressing GCaMP7s via AAV delivery. Top left: confocal image showing GCaMP7s expression in the ACC. Scale bar, 20 μm.

(B) Examples of high-frequency charge-balanced biphasic DBS waveforms: symmetric (top) and asymmetric (bottom).

(legend continued on next page)

thus offer unique advantages for resolving DBS mechanisms, enabling artifact-free, real-time monitoring of cell-specific dynamics during stimulation to accelerate next-generation protocols.

We optimized DBS parameters for precise ACC modulation in mouse depression models. Using fiber photometry of Ca^{2+} signals, we identified settings that reliably activated or inhibited ACC neurons. Inhibitory DBS (i-DBS) elicited rapid, sustained alleviation of depressive-like behaviors, while excitatory DBS (e-DBS) induced anhedonia in healthy mice. Network mapping with phosphorylated pyruvate dehydrogenase (pPDH)[19] revealed widespread inhibition across the ACC, its direct downstream targets, and several indirectly connected brain regions. These findings establish that ACC-targeted i-DBS exerts rapid antidepressant effects in mice via waveform-specific parameters, providing a mechanistic foundation for precision DBS therapy.

RESULTS

Optimization of i-DBS parameters for inhibiting ACC neurons

Building on findings that chemogenetic and optogenetic inhibition of ACC pyramidal neurons alleviates depressive-like behaviors in mice,[10,11] we first determined optimal DBS parameters for inhibiting ACC activity. We combined DBS with fiber photometry to monitor calcium/calmodulin-dependent protein kinase II (CaMKII)-expressing pyramidal neurons during stimulation (Figure 1A). Electrodes and optical fibers were implanted in the ACC, where pyramidal neurons—the primary cortical output neurons—were transduced with adeno-associated virus (AAV) encoding *CaMKII-GCaMP7s* to drive the expression of the genetically encoded calcium indicator GCaMP.[20]

We examined symmetric biphasic waveforms (50 μs interphase delay) at 130 Hz—a frequency commonly used in clinical DBS applications (Figures 1B–1G and S1A–S1D). Three parameter settings were evaluated: 200 μA–50 μs, 180 μA–100 μs, and 140 μA–140 μs (amplitude–pulse width). The 200 μA–50 μs setting elicited an initial Ca^{2+} transient without sustained inhibition (Figure 1C). The 180 μA–100 μs and 140 μA–140 μs settings induced inhibition that was weak, slow to develop, and variable across mice (Figures 1D and 1E).

To achieve faster, sustained inhibition, we tested asymmetric charge-balanced biphasic waveforms: 180–100 (180 μA–100 μs anodic/100 μA–180 μs cathodic), 160–120, and 200–80 (Figures 1H–1L and S1E–S1H). The 180–100 waveform produced immediate, robust inhibition of ACC $CaMKII^+$ neurons, evident within seconds of stimulation onset and persisting until cessation (Figures 1I and 1K–1M). This inhibition was fully reversible, indicating the safety and reliability of the protocol (Figures 1M and S1F). The 160–120 and 200–80 waveforms showed high variability and inconsistent inhibition (Figures 1H and 1J–1L).

Since DBS may excite GABAergic interneurons to inhibit pyramidal neurons,[15,21] we monitored vesicular GABA transporter$^+$ ($VGAT^+$) interneuron activity using fiber photometry in *Vgat-Cre* mice injected with *AAV-DIO-GCaMP7s* (Figure S1I). Surprisingly, both symmetric (200 μA–50 μs) and asymmetric (180–100) waveforms consistently inhibited $VGAT^+$ neurons at 15–130 Hz frequencies (Figures S1J–S1W). These results indicate DBS-induced inhibition reflects broad regional suppression rather than interneuron recruitment. Symmetric waveforms inhibited $VGAT^+$ neurons more strongly than $CaMKII^+$ neurons, suggesting GABAergic neurons are more sensitive to this waveform.

Together, these results demonstrate that the asymmetric 180–100 waveform achieves rapid, reversible, and robust inhibition of ACC pyramidal neurons without recruiting GABAergic interneurons.

Optimization of e-DBS parameters for activating ACC neurons

We next explored DBS parameters to reliably excite ACC neurons. Given that high-frequency DBS is generally associated with neuronal inhibition, while lower frequencies may facilitate excitation,[22,23] we investigated whether reducing stimulation frequency could promote activation. For symmetric biphasic waveforms (200 μA–50 μs), we tested frequencies of 5, 7, 15, and 40 Hz, and the clinically standard 130 Hz (Figures 2A–2E and S2A–S2E). Responses varied substantially across individuals, though lower frequencies trended toward exciting ACC $CaMKII^+$ neurons. At 15 Hz, significant activation occurred within the first 400 s of stimulation, but neuronal activity became inconsistent thereafter. For the asymmetric 180–100 waveform (established earlier as inhibitory at 130 Hz), stimulation at 80 and 40 Hz maintained robust, reversible inhibition (Figures 2F, 2G, S2F, and S2G). At 15 and 10 Hz, we observed a tentative excitatory trend, but effects were not statistically significant (Figures 2H–2J and S2H–S2J). These findings suggest that reducing frequency alone is insufficient for reliable ACC excitation.

To achieve stronger and more consistent excitation, we investigated whether modulating pulse width could enhance

(C–E) Effects of symmetric biphasic waveforms on ACC $CaMKII^+$ neuron activity. Top: waveform parameters: (C) 200 μA, 50 μs; (D) 140 μA, 140; and (E) 180 μA, 100 μs. Middle: heatmaps of Ca^{2+} signals ($\Delta F/F$) for individual mice, aligned to DBS onset. Bottom: average Ca^{2+} responses (n = 8, 6, and 5 mice for C, D, and E, respectively).

(F and G) Mean $\Delta F/F$ during DBS-off (−150 to −350 s) and DBS-on (800 to 1,500 s) periods (F) and area under the curve (AUC) of Ca^{2+} signals during DBS-on (G) for symmetrical stimulations. Symbols denote individual mice.

(H–J) Effects of asymmetric biphasic waveforms on ACC $CaMKII^+$ neuron activity. Top: waveform parameters are (H) 160 μA, 120 μs and −120 μA, 160 μs; (I) 180 μA, 100 μs and −100 μA, 180 μs; and (J) 200 μA, 80 μs and −80 μA, 200 μs. Middle: Ca^{2+} signal heatmaps for individual mice. Bottom: average Ca^{2+} responses (n = 5, 7, and 6 mice for H, I, and J, respectively).

(K and L) Mean $\Delta F/F$ during DBS-off and -on periods (K) and AUC of Ca^{2+} signals following DBS onset (L) for asymmetric waveforms.

(M) Example Ca^{2+} traces from ACC $CaMKII^+$ neurons during DBS with asymmetric (180–100) waveforms. Top: dynamic response heatmaps. Bottom: average Ca^{2+} signal aligned to DBS onset.

Blue and red traces represent generalized inhibitory and excitatory responses, respectively. The convention is used throughout figures. Data are presented as mean ± SEM. n.s., not significant; $^*p < 0.05$, $^{**}p < 0.01$, and $^{***}p < 0.001$. See also Figure S1 and Table S1.

activation. Extending the pulse width to 300 μs markedly improved excitatory responses in ACC CaMKII$^+$ neurons. Using a symmetric biphasic waveform (100 μA, 300 μs per phase) at 20 Hz, we achieved robust and reliable activation, with superior efficacy compared with the 15 and 130 Hz settings (Figures 2K–2O and S2K–S2M). Further analysis revealed that e-DBS, which activated ACC pyramidal neurons, also elicited activation of ACC VGAT$^+$ neurons, albeit with substantial inter-individual variability (Figures S2N and S2O).

Thus, reliable excitation requires combined adjustment of frequency and pulse width, with the symmetric 100 μA–300 μs waveform at 20 Hz emerging as an effective parameter set for activating ACC neurons.

Bidirectional ACC DBS modulates depressive-like behaviors

We assessed the behavioral effects of modulating ACC CaMKII$^+$ neurons using the optimized protocols for i-DBS (asymmetric 180 μA–100 μs/−100 μA–180 μs, 130 Hz) and e-DBS (symmetric 100 μA, 300 μs per phase, 20 Hz). First, we applied i-DBS for 2 h daily over 1 week in a chronic restraint stress (CRS) mouse model of depression,[10] in line with commonly used stimulation durations in previous mouse DBS studies[17,24–27] (Figures 3A and 3B). When tested 2 h after the final DBS session, mice that received the optimized i-DBS protocol showed a sustained reduction in immobility in the forced swim test (FST), indicating an enduring despair-reducing effect (Figures 3C and 3D). In this DBS-off condition, however, we observed no improvement in the sucrose preference test (SPT), suggesting anhedonia was not reversed without ongoing stimulation (Figures S3A–S3C).

Direct evaluation of active neuromodulation effects revealed broader therapeutic impact. Real-time i-DBS produced immediate behavioral improvements, significantly decreasing FST immobility time (Figures S3D and S3E) while concurrently enhancing sucrose preference and sucrose consumption in both the CRS model (Figures 3E, 3F, S3F, and S3G) and an independent lipopolysaccharide (LPS)-induced depression model (Figure S3J). These results reveal that ameliorating anhedonia requires online neuromodulation, whereas despair-related behaviors are improved both during and after i-DBS.

To define the therapeutic timeline, we asked how many i-DBS sessions are required to elicit sustained behavioral improvement and how long such effects persist. Remarkably, a single i-DBS session was sufficient to rescue behavioral despair both in the CRS model and in the LPS model when assessed 2 h post-stimulation (Figures 3G, 3H, S3H, and S3I). To examine the duration of this effect, we performed follow-up FSTs on days 1, 3, and 7 post-stimulation in CRS mice and found that the effect persisted for at least 3 days but was absent by day 7 (Figure 3H). Again, a single session did not improve sucrose preference (Figure S3K), confirming that the dissociation between behavioral domains is robust and not due to tolerance.

Conversely, applying daily 2-h e-DBS for 1 week in healthy, non-stressed mice induced a pronounced anhedonia-like state, measured by reduced sucrose preference (Figures 3I and 3J), without altering FST behavior (Figure 3K). This anhedonia mirrored that seen in CRS mice (Figure S3C), demonstrating that ACC hyperactivity is sufficient to drive hedonic impairment.

Neither i-DBS nor e-DBS of the ACC significantly affected locomotor activity or anxiety-like behavior compared with sham controls, as measured by the open-field test (Figure S3L) and elevated plus maze (Figure S3M). These results indicate that the primary behavioral effects—namely, alterations in sucrose preference and forced swimming immobility—are specific to mood-related domains and not confounded by changes in general mobility or anxiety, supporting the behavioral specificity and tolerability of the stimulation protocols.

ACC inhibition drives widespread network suppression

We asked how i-DBS, which alleviates depressive behaviors, might reduce neuronal activity in downstream centers. Given that c-Fos often detects activation but not inhibition, we utilized pPDH, a recently validated inverse marker of neuronal activity,[19] to map the inhibitory effects of ACC DBS at the whole-brain level.

Strong pPDH labeling indicated local ACC inhibition around the electrode, with minimal spillover to adjacent regions, confirming spatial specificity (Figure 4A). We also observed strong pPDH signals in interconnected regions: the basolateral amygdala (BLA), nucleus accumbens, ventral tegmental area, retrosplenial cortex, lateral septum, and dorsal raphe nucleus (DRN) (Figures 4B and 4C). Regions without known direct ACC projections, including the central amygdala, lateral habenula, and superior colliculus superficial gray, also showed increased pPDH labeling, suggesting propagation of inhibitory signals through secondary circuits.

We functionally validated suppression in ACC-recipient BLA neurons using fiber photometry of projection-specific Ca^{2+} signals. Anterograde transsynaptic strategy[28]—*AAV2/1-Cre* in the ACC and *AAV2/9-DIO-GCaMP7s* in the ipsilateral BLA—expressed GCaMP7s in ACC-innervated neurons. DBS electrodes and optical fibers were implanted in the ACC and BLA, respectively (Figures 4D and 4E). ACC i-DBS significantly reduced Ca^{2+} signals in BLA neurons (Figures 4F, 4G, S4A, and S4B), confirming real-time downstream suppression.

Notably, the DRN—the major source of forebrain serotonin—showed heightened pPDH sensitivity to ACC i-DBS (Figures 4A–4C). Given the established roles of serotonin and dopamine, another key monoamine, in mood regulation, we employed $GRAB_{5HT3.0}$[29] and $GRAB_{rDA3m}$[30] biosensors for real-time monoamine monitoring in the ACC (Figure S4C). ACC i-DBS robustly suppressed serotonin release under both symmetric and asymmetric protocols, with stronger effects under asymmetric stimulation (Figures S4D–S4F). Dopamine levels, however, exhibited only a transient increase during stimulation onset without sustained suppression (Figures S4G–S4I). These results identify serotonergic signaling as particularly vulnerable to DBS-mediated inhibition within the ACC.

DISCUSSION

The mechanisms underlying DBS remain enigmatic, limiting broader therapeutic application. Unlike chemogenetics or optogenetics, which afford precise control over neuronal activity, DBS's effects—whether excitatory, inhibitory, or disruptive—remain a subject of debate.[2,31] We addressed this gap using real-time fiber photometry during ACC DBS, identifying

Please cite this article in press as: Yuan et al., Optimized deep brain stimulation for anterior cingulate cortex inhibition produces antidepressant-like effects in mice, Neuron (2025), https://doi.org/10.1016/j.neuron.2025.07.018

CellPress

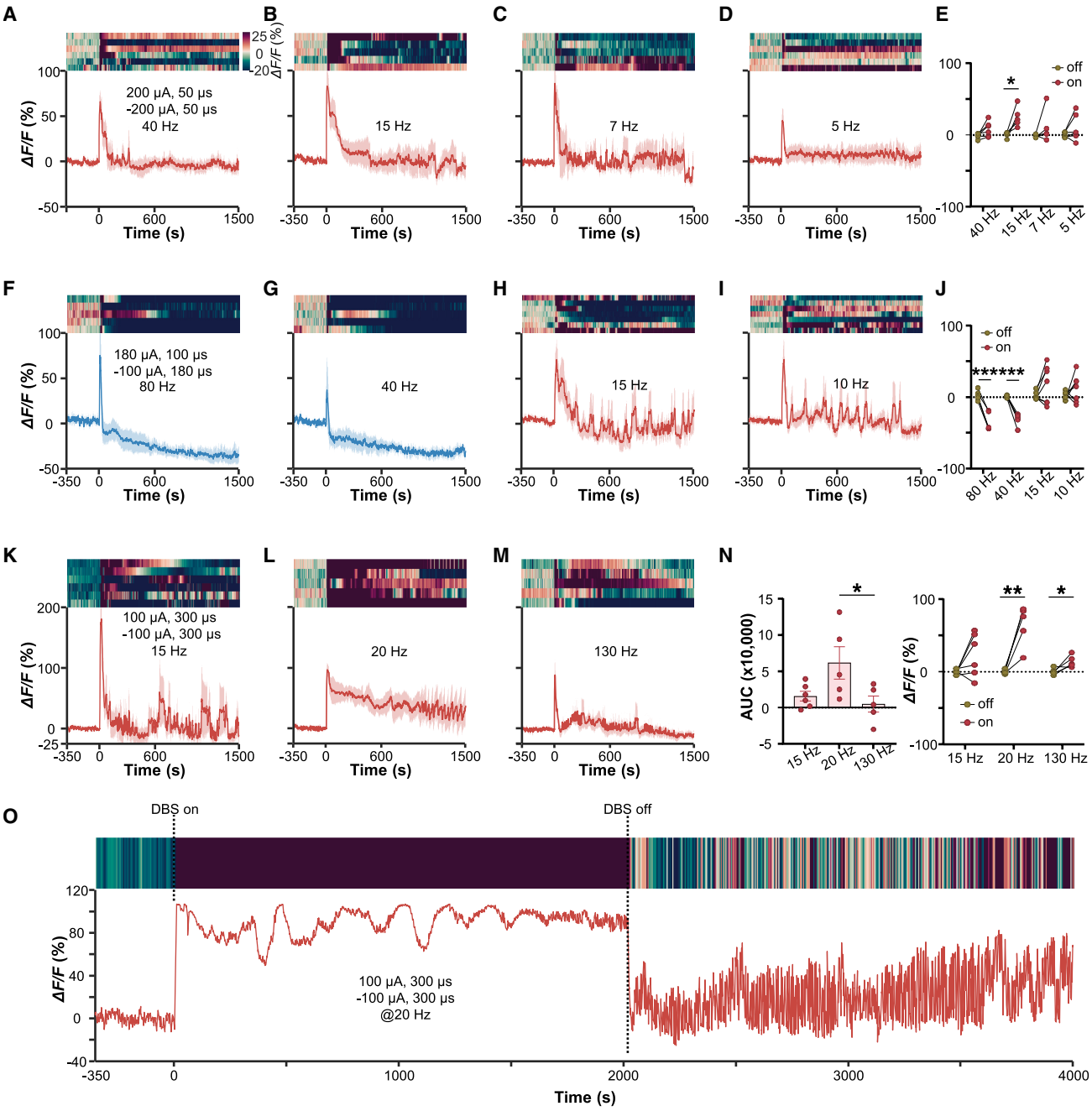

Figure 2. Identification of DBS parameters for activating ACC CaMKII$^+$ neurons

(A–D) Ca^{2+} responses ($\Delta F/F$) of ACC CaMKII$^+$ neurons to symmetric biphasic DBS (200 μA, 50 μs) at 40 Hz (A), 15 Hz (B), 7 Hz (C), and 5 Hz (D). (A, $n = 5$ or 6 mice per group.)

(E) Mean $\Delta F/F$ during DBS-off (−150 to −350 s) and DBS-on (0 to 400 s) periods for symmetric waveforms. Symbols denote individual mice.

(F–I) Ca^{2+} responses ($\Delta F/F$) asymmetric biphasic DBS (180 μA, 100 μs) at 80 Hz (F), 40 Hz (G), 15 Hz (H), and 10 Hz (I) ($n = 5$–7 mice per group).

(J) Mean $\Delta F/F$ for asymmetric DBS at varying frequencies during off- and on-stimulation periods.

(K–M) Responses to e-DBS (symmetric 100 μA, 300 μs; 50 μs inter-phase delay) at 15 Hz (K), 20 Hz (L), and 130 Hz (M). Top: response heatmaps ($n = 5$–6 mice). Bottom: average response.

(N) AUC (left) and mean $\Delta F/F$ (right) during DBS-off and -on periods for e-DBS protocols shown in (K)–(M).

(O) Example Ca^{2+} traces ($\Delta F/F$) during DBS with symmetric (100 μA, 300 μs) waveforms. Top: heatmaps of dynamic responses. Bottom: average Ca^{2+} signal curves aligned to DBS onset.

Data are presented as mean ± SEM. *$p < 0.05$, **$p < 0.01$, and ***$p < 0.001$. See also Figure S2 and Table S1.

Please cite this article in press as: Yuan et al., Optimized deep brain stimulation for anterior cingulate cortex inhibition produces antidepressant-like effects in mice, Neuron (2025), https://doi.org/10.1016/j.neuron.2025.07.018

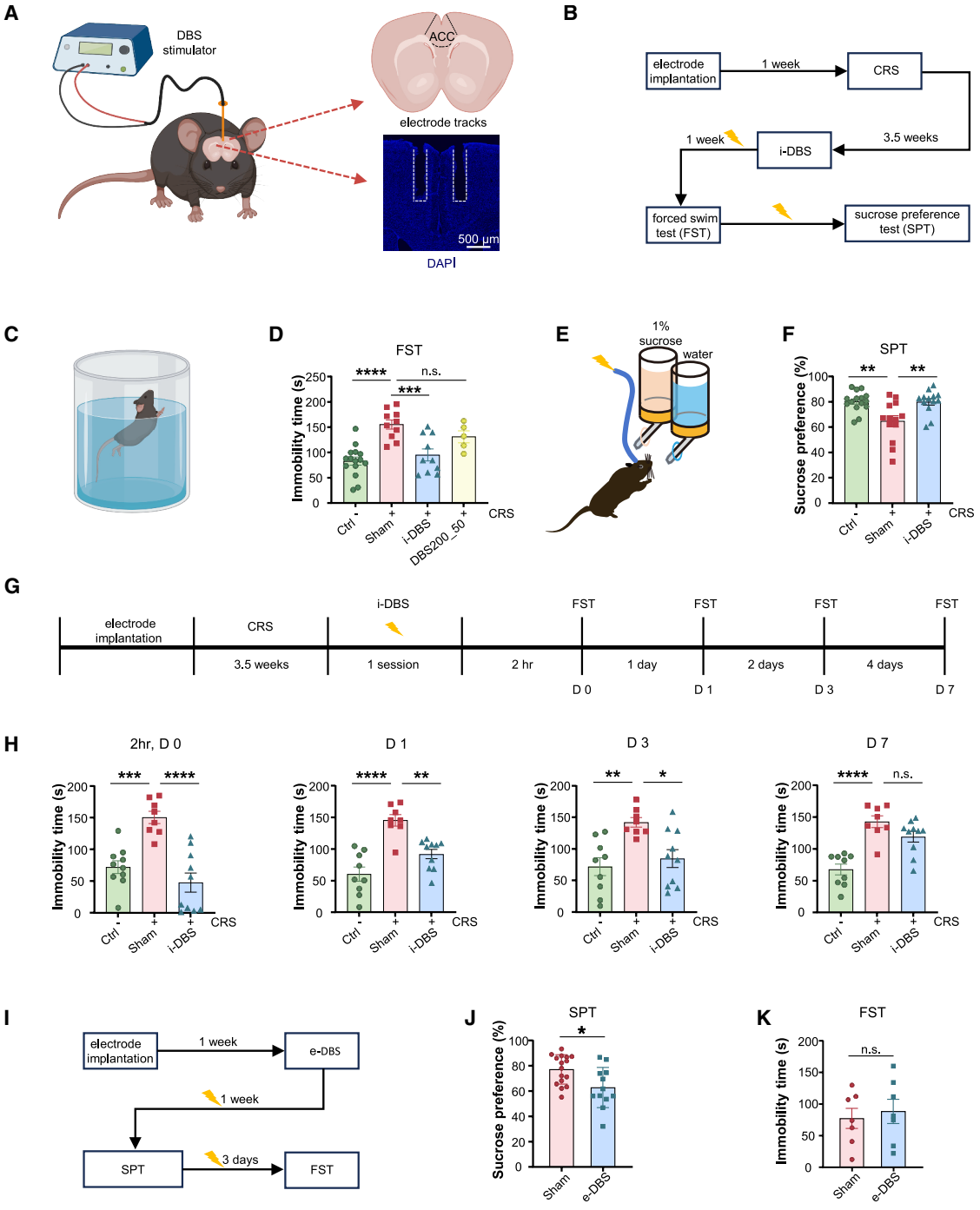

Figure 3. ACC DBS bidirectionally modulates depressive-like behaviors

(A) Schematic of bilateral DBS electrode implantation in the mouse ACC. Bottom right: representative image of an electrode track. Scale bar, 500 μm.

(B) Experimental timeline for electrode implantation, CRS, DBS, and behavioral testing.

(C) Forced swim test (FST) schematic.

(D) FST immobility time for control (Ctrl), CRS sham, and CRS mice receiving i-DBS using 180 μA, 100 μs, or 200 μA, 50 μs waveforms (n = 15, 10, 10, and 5 mice, respectively).

(E) Schematic of the sucrose preference test (SPT) with concurrent i-DBS.

(F) Sucrose preference for control (Ctrl), CRS sham, and CRS mice receiving i-DBS (180 μA, 100 μs) (n = 15, 13, and 13 mice, respectively).

(G) Experimental timeline for electrode implantation, CRS induction, single-session i-DBS, and subsequent serial FST assessments.

(legend continued on next page)

parameter sets that robustly modulate neuronal activity with minimal variability.

Our results show that DBS-induced inhibition or excitation depends on waveform symmetry, pulse width, and frequency. For inhibition, asymmetric biphasic waveforms (e.g., 180 μA, 100 μs/−100 μA, 180 μs) combined with high frequencies (80–130 Hz) reliably suppress the activity of ACC pyramidal neurons, suggesting that charge redistribution dynamics in asymmetric waveforms enhance inhibitory efficacy. For excitation, symmetric biphasic waveforms with extended pulse widths (e.g., 300 μs) at lower frequencies (15–20 Hz) promote sustained neuronal activation, likely by prolonging depolarization. Importantly, lower frequencies alone are insufficient without pulse width adjustments. These findings underscore the need for parameter balancing to achieve desired outcomes while minimizing off-target effects, suggesting a generalizable optimization strategy for circuit-specific neuromodulation.

Our data reveal a symptom-domain-specific dissociation in the persistence of ACC DBS effects: inhibitory stimulation yielded rapid, sustained reductions in behavioral despair (FST; ≥3 days), while anti-anhedonia (SPT/SCT) required ongoing stimulation. This aligns with clinical observations where continuous DBS is often essential for comprehensive benefit, though some effects may persist via neuroplasticity.[3,5] Critically, e-DBS induced anhedonia without altering despair, confirming distinct mechanistic thresholds. Reciprocal ACC connectivity with emotion-processing regions (ventral tegmental area [VTA][32] and BLA[10,33]) suggests sustained modulation may be necessary to counteract circuit-level reinforcement underlying anhedonia. These findings underscore the necessity of circuit-specific, temporally resolved intervention strategies for MDD.

Prior studies suggest two plasticity-based strategies to extend DBS benefits post-stimulation. First, adapting long-term depression protocols—where low-frequency NAc stimulation (e.g., 12 Hz) combined with D1 receptor modulation induces lasting synaptic suppression[34,35]—might persistently dampen excitatory activity. Second, structured multi-day regimens (1–2 weeks of daily sessions) modeled on NAc/BLA studies[17,24,25] may promote cumulative circuit reorganization via synaptic remodeling. These approaches reposition DBS from transient modulation toward durable, plasticity-driven antidepressant outcomes.

Building on clinical validation of SCC DBS for treatment-resistant depression,[3,4,18,36] our preclinical results identify the ACC as a promising complementary target. While SCC DBS provides clinical benefit, response variability underscores the need to explore alternative targets.[5] Our ACC-focused approach addresses this by advancing mechanism-guided neuromodulation—particularly relevant given emerging interest in other circuit-based targets like the lateral habenula,[37–39] potentially broadening precision therapies for heterogeneous MDD.

Studying DBS-induced network inhibition has been challenging. Here, we used the inverse activity marker pPDH to map inhibition elicited by ACC DBS. Key downstream areas, such as the BLA and DRN, showed elevated pPDH labeling. Notably, BLA inhibition aligns with prior evidence that the ACC-BLA circuit mediates antidepressant effects of ACC inactivation.[10] Several areas lacking direct ACC projections, such as the central amygdala and lateral habenula, also exhibited increased pPDH, suggesting multi-synaptic spread of the inhibitory signal. Despite widespread inhibition, locomotion (OFT) and anxiety-like behaviors (EPM) remained unaltered, underscoring functional specificity. Therapeutic benefits thus likely arise from targeted network modulation rather than non-selective silencing. Importantly, DRN inhibition correlated with reduced serotonin release (Figure S4). Given the role of serotonin in mood regulation,[40] combining ACC DBS with selective serotonin reuptake inhibitors (SSRIs) may enhance treatment outcomes for MDD.

In summary, our integrated framework—combining cell-type-specific monitoring with DBS parameter optimization—provides a scalable approach for cross-species validation. We demonstrate that ACC-targeted i-DBS alleviates depression-like behaviors in mice. Critically, rodent models have inherent limitations in capturing the clinical heterogeneity and treatment resistance of human MDD.[41–46] Our findings thus represent a preclinical examination of circuit-level neuromodulatory mechanisms underlying antidepressant-like responses but not direct predictors of clinical efficacy. Future systematic testing in larger brains (e.g., non-human primates) will refine protocols while de-risking translation. This strategy bridges mechanistic insights from preclinical models to actionable design principles, advancing precision neuromodulation for depression.

RESOURCE AVAILABILITY

Lead contact

Further information and requests for resources and programs should be directed to and will be fulfilled by the lead contact, Minmin Luo (luominmin@cibr.ac.cn).

Materials availability

All unique reagents generated in this study are available from the lead contact upon reasonable request.

Data and code availability

All data necessary to assess the conclusions in this manuscript are provided in the main text or the supplemental information. Any additional information is available from the corresponding authors upon request.

ACKNOWLEDGMENTS

We thank D. Yang (The Scripps Research Institute) for valuable information about pPDH staining and the Luo lab for comments. M.L. was supported by the China Brain Initiative Grant (STI2030-Major projects 2021ZD0202803), the Research Unit of Medical Neurobiology at the Chinese Academy of Medical Sciences (2019RU003), the Non-profit Central Research Institute Fund of the Chinese Academy of Medical Sciences (2024-I2M-ZD-012), the New Cornerstone Investigator Program, and the Beijing Municipal Government. Z.Y. was

(H) Lasting effects of a single i-DBS session (180 μA, 100 μs) on FST immobility at 2 h, 1 day, 3 days, and 7 days post-stimulation (n = 8–10 mice per group).
(I) Timeline for inducing depressive-like behaviors with 20 Hz e-DBS.
(J and K) Sucrose preference (J) and FST immobility (K) in sham and e-DBS mice (n = 12–16 mice for J; n = 7 mice for K).
Data are presented as mean ± SEM. n.s., not significant; $^{*}p < 0.05$, $^{**}p < 0.01$, $^{***}p < 0.001$, $^{****}p < 0.0001$. See also Figure S3 and Table S1.

Please cite this article in press as: Yuan et al., Optimized deep brain stimulation for anterior cingulate cortex inhibition produces antidepressant-like effects in mice, Neuron (2025), https://doi.org/10.1016/j.neuron.2025.07.018

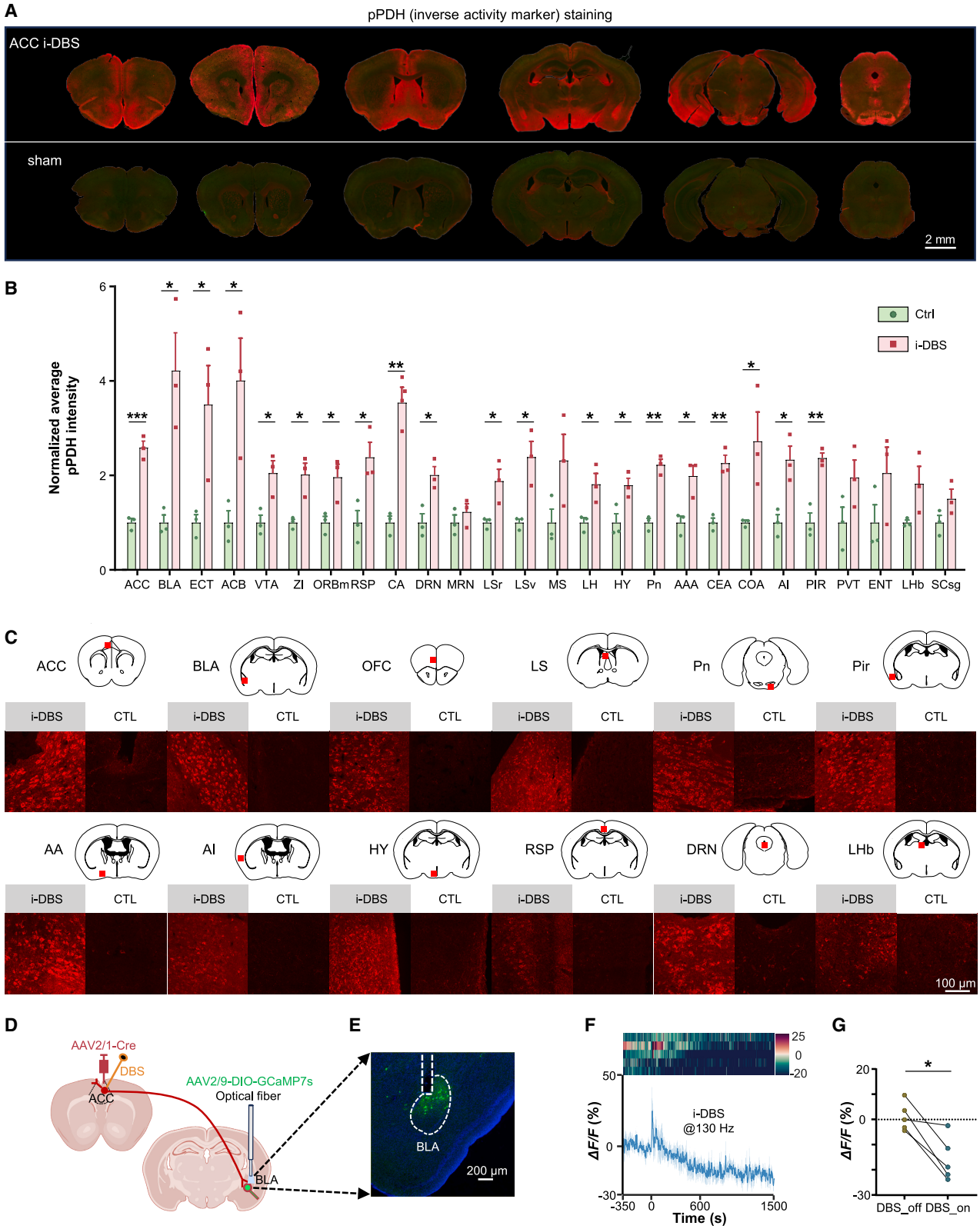

(legend on next page)

supported by the National Natural Science Foundation of China (32400820). Z.M. was supported by the China Brain Initiative Grant (2021ZD0200407).

AUTHOR CONTRIBUTIONS

Z.Y., M.L., H.Y., and Z.M. planned experiments and prepared the manuscript, with inputs from others. Z.Y., H.Y., P.W., and X.H. conducted behavioral tests and recordings. Z.M. and J.Z. established the DBS setup. R.D. constructed the AAV2/9-CaMKII-GCaMP7s vector. Y.L. developed the $GRAB_{5HT3.0}$ and $GRAB_{rDA3m}$ sensors. K.X. and Y.Z. conducted electrophysiology recording. Y.G., X.G., and Q.G. helped with microscopic imaging and pPDH labeling quantification.

DECLARATION OF INTERESTS

M.L. serves on *Neuron*'s scientific advisory board.

STAR★METHODS

Detailed methods are provided in the online version of this paper and include the following:

- KEY RESOURCES TABLE
- EXPERIMENTAL MODEL AND SUBJECT DETAILS
- METHOD DETAILS
  - Viral vectors
  - Surgery
  - Chronic restraint stress (CRS)
  - Lipopolysaccharide (LPS) - induced depression model
  - Sucrose preference test (SPT)
  - Sucrose consumption test (SCT)
  - Forced swim test (FST)
  - Elevated plus maze (EPM)
  - Open field test (OFT)
  - *In vivo* fiber photometry
  - DBS treatment
  - Immunohistochemistry
  - pPDH imaging and quantification
- QUANTIFICATION AND STATISTICAL ANALYSIS

SUPPLEMENTAL INFORMATION

Supplemental information can be found online at https://doi.org/10.1016/j.neuron.2025.07.018.

Received: February 7, 2025
Revised: June 9, 2025
Accepted: July 16, 2025

REFERENCES

1. Sandoval-Pistorius, S.S., Hacker, M.L., Waters, A.C., Wang, J., Provenza, N.R., de Hemptinne, C., Johnson, K.A., Morrison, M.A., and Cernera, S. (2023). Advances in Deep Brain Stimulation: From Mechanisms to Applications. J. Neurosci. *43*, 7575–7586. https://doi.org/10.1523/JNEUROSCI.1427-23.2023.
2. Gilbert, Z., Mason, X., Sebastian, R., Tang, A.M., Martin Del Campo-Vera, R., Chen, K.-H., Leonor, A., Shao, A., Tabarsi, E., Chung, R., et al. (2023). A review of neurophysiological effects and efficiency of waveform parameters in deep brain stimulation. Clin. Neurophysiol. *152*, 93–111. https://doi.org/10.1016/j.clinph.2023.04.007.
3. Mayberg, H.S., Lozano, A.M., Voon, V., McNeely, H.E., Seminowicz, D., Hamani, C., Schwalb, J.M., and Kennedy, S.H. (2005). Deep brain stimulation for treatment-resistant depression. Neuron *45*, 651–660. https://doi.org/10.1016/j.neuron.2005.02.014.
4. Johnson, K.A., Okun, M.S., Scangos, K.W., Mayberg, H.S., and de Hemptinne, C. (2024). Deep brain stimulation for refractory major depressive disorder: a comprehensive review. Mol. Psychiatry *29*, 1075–1087. https://doi.org/10.1038/s41380-023-02394-4.
5. Holtzheimer, P.E., Husain, M.M., Lisanby, S.H., Taylor, S.F., Whitworth, L. A., McClintock, S., Slavin, K.V., Berman, J., McKhann, G.M., Patil, P.G., et al. (2017). Subcallosal cingulate deep brain stimulation for treatment-resistant depression: a multisite, randomised, sham-controlled trial. Lancet Psychiatry *4*, 839–849. https://doi.org/10.1016/S2215-0366(17)30371-1.
6. Barthas, F., Humo, M., Gilsbach, R., Waltisperger, E., Karatas, M., Leman, S., Hein, L., Belzung, C., Boutillier, A.-L., Barrot, M., et al. (2017). Cingulate overexpression of mitogen-activated protein kinase phosphatase-1 as a key factor for depression. Biol. Psychiatry *82*, 370–379. https://doi.org/10.1016/j.biopsych.2017.01.019.
7. Diener, C., Kuehner, C., Brusniak, W., Ubl, B., Wessa, M., and Flor, H. (2012). A meta-analysis of neurofunctional imaging studies of emotion and cognition in major depression. NeuroImage *61*, 677–685. https://doi.org/10.1016/j.neuroimage.2012.04.005.
8. Holmes, S.E., Hinz, R., Conen, S., Gregory, C.J., Matthews, J.C., Anton-Rodriguez, J.M., Gerhard, A., and Talbot, P.S. (2018). Elevated translocator protein in anterior cingulate in major depression and a role for inflammation in suicidal thinking: A positron emission tomography study. Biol. Psychiatry *83*, 61–69. https://doi.org/10.1016/j.biopsych.2017.08.005.
9. Alexander, L., Jelen, L.A., Mehta, M.A., and Young, A.H. (2021). The anterior cingulate cortex as a key locus of ketamine's antidepressant action. Neurosci. Biobehav. Rev. *127*, 531–554. https://doi.org/10.1016/j.neubiorev.2021.05.003.
10. Yuan, Z., Qi, Z., Wang, R., Cui, Y., An, S., Wu, G., Feng, Q., Lin, R., Dai, R., Li, A., et al. (2023). A corticoamygdalar pathway controls reward

Figure 4. ACC-targeted i-DBS suppresses neural activity in widespread brain networks

(A) Whole-brain pPDH immunolabeling 15 min after ACC i-DBS (asymmetric 180 μA, 100 μs). Red, pPDH (Cy3); green, autofluorescence for anatomical context. Scale bar, 2 mm.

(B) Quantification of pPDH signal intensity across select brain regions (n = 3 mice per group).

(C) Representative confocal images of pPDH labeling. Scale bar, 100 μm.

(D) Schematic of fiber photometry of Ca^{2+} dynamics from ACC-recipient BLA neurons during ACC DBS.

(E) Representative coronal section showing GCaMP7s expression in ACC-recipient BLA neurons and the optical fiber track. DAPI (blue) counterstains nuclei. Scale bar, 200 μm.

(F) Applying i-DBS (130 Hz, asymmetric 180 μA, 100 μs) in the ACC suppresses Ca^{2+} activity in ACC-recipient BLA neurons (n = 5 mice). Top: response heatmaps. Bottom: average Ca^{2+} trace aligned to DBS onset.

(G) Mean $\Delta F/F$ of Ca^{2+} signals in BLA neurons during DBS-off and -on periods. Symbols represent individual mice.

Abbreviations: ECT, ectorhinal area; ACB, nucleus accumbens; VTA, ventral tegmental area; ZI, zona incerta; ORBm, orbital area, medial part; RSP, retrosplenial area; MRN, median raphe nucleus; LSr, lateral septal nucleus, rostral part; LSv, lateral septal nucleus, ventral part; MS, medial septal nucleus; LH, lateral hypothalamus; HY, hypothalamus; Pn, pontine nucleus; AA, anterior amygdala; CeA, central amygdala; CoA, cortical amygdala; AI, agranular insular; PIR, piriform; PVT, paraventricular nucleus of thalamus; ENT, entorhinal area; LHb, lateral habenula; SCsg, superior colliculus, superficial gray. Data are presented as mean ± SEM. $^{*}p < 0.05$, $^{**}p < 0.01$, and $^{***}p < 0.001$. See also Figure S4 and Table S1.

devaluation and depression using dynamic inhibition code. Neuron *111*, 3837–3853.e5. https://doi.org/10.1016/j.neuron.2023.08.022.

11. Sellmeijer, J., Mathis, V., Hugel, S., Li, X.-H., Song, Q., Chen, Q.-Y., Barthas, F., Lutz, P.-E., Karatas, M., Luthi, A., et al. (2018). Hyperactivity of anterior cingulate cortex areas 24a/24b drives chronic pain-induced anxiodepressive-like consequences. J. Neurosci. *38*, 3102–3115. https://doi.org/10.1523/JNEUROSCI.3195-17.2018.
12. Fitzgerald, P.B., and Segrave, R.A. (2015). Deep brain stimulation in mental health: Review of evidence for clinical efficacy. Aust. N. Z. J. Psychiatry *49*, 979–993. https://doi.org/10.1177/0004867415598011.
13. Vissani, M., Isaias, I.U., and Mazzoni, A. (2020). Deep brain stimulation: a review of the open neural engineering challenges. J. Neural Eng. *17*, 051002. https://doi.org/10.1088/1741-2552/abb581.
14. Deep-Brain Stimulation; Parkinson's; Disease Study Group, Obeso, J.A., Olanow, C.W., Rodriguez-Oroz, M.C., Krack, P., Kumar, R., and Lang, A.E. (2001). Deep-Brain Stimulation of the Subthalamic Nucleus or the Pars Interna of the Globus Pallidus in Parkinson's Disease. N. Engl. J. Med. *345*, 956–963. https://doi.org/10.1056/NEJMoa000827.
15. Lin, Z.-J., Gu, X., Gong, W.-K., Wang, M., Wu, Y.-J., Wang, Q., Wu, X.-R., Zhao, X.-Y., Zhu, M.X., Wang, L.-Y., et al. (2024). Stimulation of an entorhinal-hippocampal extinction circuit facilitates fear extinction in a post-traumatic stress disorder model. J. Clin. Invest. *134*, e181095. https://doi.org/10.1172/JCI181095.
16. Lowet, E., Kondabolu, K., Zhou, S., Mount, R.A., Wang, Y., Ravasio, C.R., and Han, X. (2022). Deep brain stimulation creates informational lesion through membrane depolarization in mouse hippocampus. Nat. Commun. *13*, 7709. https://doi.org/10.1038/s41467-022-35314-1.
17. Gao, Y., Gao, D., Zhang, H., Zheng, D., Du, J., Yuan, C., Ma, M., Yin, Y., Wang, J., Zhang, X., et al. (2024). BLA DBS improves anxiety and fear by correcting weakened synaptic transmission from BLA to adBNST and CeL in a mouse model of foot shock. Cell Rep. *43*, 113766. https://doi.org/10.1016/j.celrep.2024.113766.
18. Alagapan, S., Choi, K.S., Heisig, S., Riva-Posse, P., Crowell, A., Tiruvadi, V., Obatusin, M., Veerakumar, A., Waters, A.C., Gross, R.E., et al. (2023). Cingulate dynamics track depression recovery with deep brain stimulation. Nature *622*, 130–138. https://doi.org/10.1038/s41586-023-06541-3.
19. Yang, D., Wang, Y., Qi, T., Zhang, X., Shen, L., Ma, J., Pang, Z., Lal, N.K., McClatchy, D.B., Seradj, S.H., et al. (2024). Phosphorylation of pyruvate dehydrogenase inversely associates with neuronal activity. Neuron *112*, 959–971.e8. https://doi.org/10.1016/j.neuron.2023.12.015.
20. Bekkers, J.M. (2011). Pyramidal neurons. Curr. Biol. *21*, R975. https://doi.org/10.1016/j.cub.2011.10.037.
21. Valverde, S., Vandecasteele, M., Piette, C., Derousseaux, W., Gangarossa, G., Aristieta Arbelaiz, A., Touboul, J., Degos, B., and Venance, L. (2020). Deep brain stimulation-guided optogenetic rescue of parkinsonian symptoms. Nat. Commun. *11*, 2388. https://doi.org/10.1038/s41467-020-16046-6.
22. Benabid, A.L., Benazzous, A., and Pollak, P. (2002). Mechanisms of deep brain stimulation. Mov. Disord. *17*, S73–S74. https://doi.org/10.1002/mds.10145.
23. Zhang, M., Yang, L., Li, Z., Fei, F., Zhou, Y., Jiang, D., Zheng, Y., Cheng, H., Wang, Y., Xu, C., et al. (2024). Low-frequency stimulation in the zona incerta attenuates seizure via driving GABAergic neuronal activity. Neurobiol. Dis. *192*, 106424. https://doi.org/10.1016/j.nbd.2024.106424.
24. Gong, W.-K., Li, X., Wang, L., Yang, Q., Tiran-Cappello, A., Liang, Z., Samsom, J., Liu, Q., Lin, H., Baunez, C., et al. (2025). Prefrontal FGF1 Signaling is Required for Accumbal Deep Brain Stimulation Treatment of Addiction. Adv. Sci. (Weinh) *12*, e2413370. https://doi.org/10.1002/advs.202413370.
25. Song, N., Liu, Z., Gao, Y., Lu, S., Yang, S., and Yuan, C. (2024). NAc-DBS corrects depression-like behaviors in CUMS mouse model via disinhibition of DA neurons in the VTA. Mol. Psychiatry *29*, 1550–1566. https://doi.org/10.1038/s41380-024-02476-x.
26. Dournes, C., Beeské, S., Belzung, C., and Griebel, G. (2013). Deep brain stimulation in treatment-resistant depression in mice: Comparison with the CRF1 antagonist, SSR125543. Prog. Neuropsychopharmacol. Biol. Psychiatry *40*, 213–220. https://doi.org/10.1016/j.pnpbp.2012.07.019.
27. Schmuckermair, C., Gaburro, S., Sah, A., Landgraf, R., Sartori, S.B., and Singewald, N. (2013). Behavioral and Neurobiological Effects of Deep Brain Stimulation in a Mouse Model of High Anxiety- and Depression-Like Behavior. Neuropsychopharmacology *38*, 1234–1244. https://doi.org/10.1038/npp.2013.21.
28. Zingg, B., Chou, X.L., Zhang, Z.G., Mesik, L., Liang, F., Tao, H.W., and Zhang, L.I. (2017). AAV-Mediated Anterograde Transsynaptic Tagging: Mapping Corticocollicular Input-Defined Neural Pathways for Defense Behaviors. Neuron *93*, 33–47. https://doi.org/10.1016/j.neuron.2016.11.045.
29. Deng, F., Wan, J., Li, G., Dong, H., Xia, X., Wang, Y., Li, X., Zhuang, C., Zheng, Y., Liu, L., et al. (2024). Improved green and red GRAB sensors for monitoring spatiotemporal serotonin release in vivo. Nat. Methods *21*, 692–702. https://doi.org/10.1038/s41592-024-02188-8.
30. Zhuo, Y., Luo, B., Yi, X., Dong, H., Miao, X., Wan, J., Williams, J.T., Campbell, M.G., Cai, R., Qian, T., et al. (2024). Improved green and red GRAB sensors for monitoring dopaminergic activity in vivo. Nat. Methods *21*, 680–691. https://doi.org/10.1038/s41592-023-02100-w.
31. Choi, K.S., and Mayberg, H. (2022). Connectomic DBS in major depression. Chapter 20. In Connectomic Deep Brain Stimulation, A. Horn, ed. (Academic Press), pp. 433–447. https://doi.org/10.1016/B978-0-12-821861-7.00022-1.
32. Song, Q., Wei, A., Xu, H., Gu, Y., Jiang, Y., Dong, N., Zheng, C., Wang, Q., Gao, M., Sun, S., et al. (2024). An ACC–VTA–ACC positive-feedback loop mediates the persistence of neuropathic pain and emotional consequences. Nat. Neurosci. *27*, 272–285. https://doi.org/10.1038/s41593-023-01519-w.
33. Kim, S.-W., Kim, M., Baek, J., Latchoumane, C.-F., Gangadharan, G., Yoon, Y., Kim, D.-S., Lee, J.H., and Shin, H.-S. (2023). Hemispherically lateralized rhythmic oscillations in the cingulate-amygdala circuit drive affective empathy in mice. Neuron *111*, 418–429.e4. https://doi.org/10.1016/j.neuron.2022.11.001.
34. Creed, M., Pascoli, V.J., and Lüscher, C. (2015). Addiction therapy. Refining deep brain stimulation to emulate optogenetic treatment of synaptic pathology. Science *347*, 659–664. https://doi.org/10.1126/science.1260776.
35. Lüscher, C., and Pollak, P. (2016). Optogenetically inspired deep brain stimulation: linking basic with clinical research. Swiss Med. Wkly. *146*, w14278. https://doi.org/10.4414/smw.2016.14278.
36. Ramasubbu, R., Anderson, S., Haffenden, A., Chavda, S., and Kiss, Z.H.T. (2013). Double-blind optimization of subcallosal cingulate deep brain stimulation for treatment-resistant depression: a pilot study. J. Psychiatry Neurosci. *38*, 325–332. https://doi.org/10.1503/jpn.120160.
37. Germann, J., Mameli, M., Elias, G.J.B., Loh, A., Taha, A., Gouveia, F.V., Boutet, A., and Lozano, A.M. (2021). Deep Brain Stimulation of the Habenula: Systematic Review of the Literature and Clinical Trial Registries. Front. Psychiatry *12*, 730931. https://doi.org/10.3389/fpsyt.2021.730931.
38. Wang, Z., Jiang, C., Guan, L., Zhao, L., Fan, T., Wang, J., Cai, X., Zhang, Y., Yao, C., Peng, B., et al. (2024). Deep brain stimulation of habenula reduces depressive symptoms and modulates brain activities in treatment-resistant depression. Nat. Mental Health *2*, 1045–1052. https://doi.org/10.1038/s44220-024-00286-2.
39. Meng, H., Wang, Y., Huang, M., Lin, W., Wang, S., and Zhang, B. (2011). Chronic deep brain stimulation of the lateral habenula nucleus in a rat model of depression. Brain Res. *1422*, 32–38. https://doi.org/10.1016/j.brainres.2011.08.041.
40. Moncrieff, J., Cooper, R.E., Stockmann, T., Amendola, S., Hengartner, M.P., and Horowitz, M.A. (2023). The serotonin theory of depression: a

systematic umbrella review of the evidence. Mol. Psychiatry *28*, 3243–3256. https://doi.org/10.1038/s41380-022-01661-0.

41. American Psychiatric Association (2013). Diagnostic and Statistical Manual of Mental Disorders (DSM-5®) (American Psychiatric Publishers).
42. Cryan, J.F., Markou, A., and Lucki, I. (2002). Assessing antidepressant activity in rodents: recent developments and future needs. Trends Pharmacol. Sci. *23*, 238–245. https://doi.org/10.1016/S0165-6147(02)02017-5.
43. Yankelevitch-Yahav, R., Franko, M., Huly, A., and Doron, R. (2015). The Forced Swim Test as a Model of Depressive-like Behavior. J. Vis. Exp. 52587. https://doi.org/10.3791/52587.
44. Liu, M.-Y., Yin, C.-Y., Zhu, L.-J., Zhu, X.-H., Xu, C., Luo, C.-X., Chen, H., Zhu, D.-Y., and Zhou, Q.-G. (2018). Sucrose preference test for measurement of stress-induced anhedonia in mice. Nat. Protoc. *13*, 1686–1698. https://doi.org/10.1038/s41596-018-0011-z.
45. Gururajan, A., Reif, A., Cryan, J.F., and Slattery, D.A. (2019). The future of rodent models in depression research. Nat. Rev. Neurosci. *20*, 686–701. https://doi.org/10.1038/s41583-019-0221-6.
46. Planchez, B., Surget, A., and Belzung, C. (2019). Animal models of major depression: drawbacks and challenges. J. Neural Transm. (Vienna) *126*, 1383–1408. https://doi.org/10.1007/s00702-019-02084-y.
47. Lin, R., Liang, J., Wang, R., Yan, T., Zhou, Y., Liu, Y., Feng, Q., Sun, F., Li, Y., Li, A., et al. (2020). The raphe dopamine system controls the expression of incentive memory. Neuron *106*, 498–514.e8. https://doi.org/10.1016/j.neuron.2020.02.009.
48. Kim, K.-S., and Han, P.-L. (2006). Optimization of chronic stress paradigms using anxiety- and depression-like behavioral parameters. J. Neurosci. Res. *83*, 497–507. https://doi.org/10.1002/jnr.20754.
49. O'Connor, J.C., Lawson, M.A., André, C., Moreau, M., Lestage, J., Castanon, N., Kelley, K.W., and Dantzer, R. (2009). Lipopolysaccharide-induced depressive-like behavior is mediated by indoleamine 2,3-dioxygenase activation in mice. Mol. Psychiatry *14*, 511–522. https://doi.org/10.1038/sj.mp.4002148.
50. Yin, R., Zhang, K., Li, Y., Tang, Z., Zheng, R., Ma, Y., Chen, Z., Lei, N., Xiong, L., Guo, P., et al. (2023). Lipopolysaccharide-induced depression-like model in mice: meta-analysis and systematic evaluation. Front. Immunol. *14*, 1181973. https://doi.org/10.3389/fimmu.2023.1181973.
51. Rodriguez, A., Zhang, H., Klaminder, J., Brodin, T., Andersson, P.L., and Andersson, M. (2018). ToxTrac: A fast and robust software for tracking organisms. Methods Ecol. Evol. *9*, 460–464. https://doi.org/10.1111/2041-210X.12874.
52. Li, Y., Zhong, W., Wang, D., Feng, Q., Liu, Z., Zhou, J., Jia, C., Hu, F., Zeng, J., Guo, Q., et al. (2016). Serotonin neurons in the dorsal raphe nucleus encode reward signals. Nat. Commun. *7*, 10503. https://doi.org/10.1038/ncomms10503.
53. Wang, Q., Ding, S.-L., Li, Y., Royall, J., Feng, D., Lesnar, P., Graddis, N., Naeemi, M., Facer, B., Ho, A., et al. (2020). The allen mouse brain common coordinate framework: A 3D reference atlas. Cell *181*, 936–953.e20. https://doi.org/10.1016/j.cell.2020.04.007.
54. Chiaruttini, N., Castoldi, C., Requie, L.M., Camarena-Delgado, C., Bianco, B. dal, Gräff, J., Seitz, A., and Silva, B.A. (2024). ABBA, a novel tool for whole-brain mapping, reveals brain-wide differences in immediate early genes induction following learning. Preprint at bioRxiv. https://doi.org/10.1101/2024.09.06.611625.
55. Bankhead, P., Loughrey, M.B., Fernández, J.A., Dombrowski, Y., McArt, D.G., Dunne, P.D., McQuaid, S., Gray, R.T., Murray, L.J., Coleman, H.G., et al. (2017). QuPath: Open source software for digital pathology image analysis. Sci. Rep. *7*, 16878. https://doi.org/10.1038/s41598-017-17204-5.

Please cite this article in press as: Yuan et al., Optimized deep brain stimulation for anterior cingulate cortex inhibition produces antidepressant-like effects in mice, Neuron (2025), https://doi.org/10.1016/j.neuron.2025.07.018

STAR★METHODS

KEY RESOURCES TABLE

REAGENT or RESOURCE	SOURCE	IDENTIFIER
Antibodies		
Recombinant Anti-NeuN antibody	Abcam	Cat#ab177487; RRID:AB_2532109
Anti-PDH-E1a (pSer293) Rabbit mAb	Cell Signaling Technology	Cat#37115S; RRID: AB_2923272
Goat anti-rabbit-Cy3	Jackson ImmunoResearch	Cat#111-165-008; RRID:AB_2338002
Bacterial and virus strains		
AAV2/9-EF1a-DIO-GCaMP7s	CIBR Vector Core	N/A
AAV2/9-CaMKIIa-GCaMP7s	Minmin Luo lab	N/A
scAAV2/1-hsyn-Cre	Taitool	Cat#S0292-1
AAV2/9-hsyn-GRAB5HT3.0	Yulong Li lab (Peking University)	N/A
AAV2/9-hsyn-GRABrDA3m	Yulong Li lab (Peking University)	N/A
Chemicals, peptides, and recombinant proteins		
LPS O127:B8	Sigma-Aldrich	Cat#L3129
Experimental models: Organisms/strains		
Mouse: Vgat-Cre	The Jackson Laboratory	Cat#028862; RRID:IMSR_JAX:028862
Mouse: C57BL/6J	Beijing Vital River Laboratory Animal Technology Co., Ltd. (China)	Cat#219
Software and algorithms		
MATLAB R2020a	MathWorks	https://www.mathworks.com
GraphPad Prism 8	GraphPad	https://www.graphpad.com/
OlyVIA 2.7	Olympus	https://olyvia.software.informer.com/
ImageJ (FIJI) (version 2.1.0)	NIH	https://imagej.net/software/fiji/
QuPath (v0.5.1)	OpenSource	https://qupath.github.io/
Other		
Fiber photometry system	Nanjing ThinkerTech	N/A
DBS system	Zhejiang University	N/A

EXPERIMENTAL MODEL AND SUBJECT DETAILS

Animal care and use strictly followed the approval of the Animal Care and Use Committee of the Chinese Institute for Brain Research, Beijing (Approval ID: CIBR-IACUC-001) in accordance with the Regulations for the Administration of Affairs Concerning Experimental Animals of China. We obtained *Vgat-Cre* mice (JAX Strain 028862) from Jackson Laboratory and purchased C57BL/6J mice from Vital River (Beijing, China). We used mice aged 7–20 weeks for our experiments. Mice were housed in groups of no more than five under a reverse 12/12 light/dark cycle, with *ad libitum* access to food and water. All experiments were conducted during the dark phase.

METHOD DETAILS

Viral vectors

AAV vectors *rAAV2/9-hsyn-GRAB5HT3.0* (simplified as *rAAV-hsyn-GRAB5HT3.0*), *rAAV2/9-hsyn-GRABrDA3m* (simplified as *rAAV-hsyn-GRABrDA3m*), *rAAV2/9-EF1a-DIO-GCaMP7s* (simplified as *rAAV-DIO-GCaMP7s*), *rAAV2/9-CaMKII-GCaMP7s* (simplified as *rAAV-CaMKII-GCaMP7s*), were packaged with titers of 1–10 $\times$ 10^{12} viral genomes (v.g.) ·mL^{-1} as previously described.[47] scAAV2/1-hSyn-Cre (3.6 $\times$ 10^{12} viral genomes v.g. ·mL^{-1}, simplified as *AAV2/1-Cre*) were purchased from Shanghai Taitool Bioscience Co., China.

Surgery

Mice were anesthetized with Avertin (i.p., 250 mg·kg^{-1}) and mounted to a stereotaxic apparatus (RWD Co., China). A small craniotomy above the ACC was made. AAV vectors (300 nL) were injected from the craniotomy by a microsyringe pump (nanoliter 2000 Injector, WPI) under a slow velocity of 46 nl·min^{-1}. The following stereotaxic coordinates were used to target the ACC and the BLA [anterior-posterior (AP), medial-lateral (ML), dorsal-ventral (DV) in the unit of mm from the bregma]: ACC (+1.18, ± 0.30, -1.7∼-1.8); BLA (-1.22, ± 3.20, -4.95). Optical fibers or DBS electrodes were implanted on the same AAV vector injection sites in the ACC or the BLA.

Chronic restraint stress (CRS)

We challenged mice with restraint stress by placing mice into a 50-ml conical tube individually for 3 to 5 hours per day, lasting 3.5 weeks. The tube was drilled to ensure air circulation, and a 3 cm cylinder was plugged into the end of the tube to make the mouse completely immobile. The control mice were group-housed in their home cage without any disturbance.[48]

Lipopolysaccharide (LPS) - induced depression model

Male C57BL/6J mice were intraperitoneally injected with lipopolysaccharide (LPS; 1 mg/kg, serotype O127:B8; 0.1 mg/mL in sterile saline) to induce an acute depressive-like state.[49,50] Control mice received an equivalent volume of sterile saline. The inhibitory ACC DBS was applied between 24 and 26 hours after LPS injection. The forced swim test (FST) was conducted at 28 hours post-LPS, two hours after the cessation of DBS. The sucrose preference test (SPT) was performed at 48 hours post-LPS under continuous inhibitory ACC DBS.

Sucrose preference test (SPT)

Mice were presented with one bottle of 1% sucrose and one bottle of pure water in their homecages for two days to acclimate before the test. On the test day, mice were singly housed in a chamber with two bottles, one filled with 1% sucrose and the other with pure water. We measured the weight difference of the two bottles respectively after 4 hours. The sucrose preference was determined by calculating the percentage of sucrose intake over the total weight of water and sucrose intake by mice.

Sucrose consumption test (SCT)

Mice were individually placed in a testing chamber equipped with a DBS system, which was employed to bilaterally inhibit the anterior cingulate cortex (ACC) using specified stimulation parameters. A bottle containing a 2% sucrose solution was provided for a 2-hour period, during which the DBS stimulation was continuously administered.

Forced swim test (FST)

We put mice individually into Plexiglass cylinders (26.5 cm height × 18 cm diameter) with 14 cm water (25±1°C) filled in. The test lasted 6 minutes under normal illumination with a digital video camera recording from the side. Only the immobility time (which was defined as the time when mice floated passively without any movements other than the necessary ones to keep their bodies balanced) during the 3rd - 6th minutes of the test was scored by a trained observer.

Elevated plus maze (EPM)

The EPM test was conducted using a standard apparatus consisting of two open arms (35 cm × 5 cm), two closed arms (35 cm × 5 cm), and a central platform (5 cm × 5 cm), elevated 50 cm above the floor. Behavioral activity was recorded using an overhead camera and analyzed with EthoVision XT 16 software (Noldus Information Technology). Mice were first habituated to the testing room for 2 hours prior to the experiment. Following habituation, mice were connected to the DBS apparatus and placed at the center of the maze facing one of the open arms. To minimize potential confounds from transient stimulation effects, mice in the i-DBS group were introduced into the maze 1 minute after DBS onset. In contrast, mice in the e-DBS and sham groups were placed in the maze immediately upon stimulation onset. The number of entries into, and the time spent in, both the open and closed arms were quantified as primary measures of anxiety-like behavior. Additionally, total distance traveled during the test was recorded as a measure of general locomotor activity.

Open field test (OFT)

Mice were gently placed into a square chamber (length 56 × width 56 × height 30, in cm) for 10 min with an overhead video camera recording the activity of the mice above the chamber. The route and distance were analyzed by ToxTrac.[51] Similarly, to minimize potential confounds from transient stimulation effects, mice in the i-DBS group were introduced into the chamber 1 minute after DBS onset.

In vivo fiber photometry

The procedure for fiber photometry recording was performed as previously described.[52] Briefly, we implanted an optical fiber in the ACC following the injection of different vectors (including *rAAV-DIO-GCaMP7s, rAAV-CaMKII-GCaMP7s, rAAV-hsyn-GRAB5HT3.0, rAAV-hsyn-GRABrDA3m*) at the same site. It is important to note that the DBS electrode was also positioned at this precise location, allowing for the concomitant application of DBS therapy and optical calcium recording. The optical fiber was attached to the skull of

Please cite this article in press as: Yuan et al., Optimized deep brain stimulation for anterior cingulate cortex inhibition produces antidepressant-like effects in mice, Neuron (2025), https://doi.org/10.1016/j.neuron.2025.07.018

mice by dental cement. After two weeks for the expression of sensors, we recorded the fluorescence signals during different behavioral tests. For trans-synaptic recordings targeting ACC-innervated BLA neurons, AAV2/1-*Cre* and AAV2/9-DIO-GCaMP7s were allowed to express for at least three weeks to ensure robust labeling. We used the multi-channel fiber photometry system (ThinkerTech, Nanjing, China) to record fluorescence signals emanating from the mouse brain. The laser power was restricted to ~20 μW at the fiber tip to minimize fluorescence bleaching. The values of fluorescence change ($\Delta F/F$) were determined by calculating $(F - F_0)/F_0$, where F_0 is the baseline fluorescence signal averaged over a 2 s-long control time window, typically preceding the trigger events (i.e. -2 – 0 s). To facilitate intuitive visualization of photometry traces, we used a color scheme in which blue and red lines represent conditions generally associated with inhibitory-like and excitatory-like trends, respectively. This scheme is intended to guide interpretation.

DBS treatment

The bipolar DBS electrodes utilized in this study were composed of nickel-cadmium material, with each individual electrode wire having a diameter of 75 μm. Each stimulation site was equipped with two such electrode wires twisted together in a helical configuration, resulting in an overall diameter of 150 μm. Electrical stimulation was delivered via a custom-made isolated pulse stimulator, with stimulation patterns triggered by a custom MATLAB program. All waveforms employed in this study were charge-balanced biphasic waveforms, featuring a 50 μs inter-phase interval. The waveforms used can be categorized into symmetric and asymmetric types, with specific parameters as follows:

Symmetric Waveforms

anodic phase 200 μA, 50 μs and cathodic phase -200 μA, 50 μs; anodic phase 140 μA, 140 μs and cathodic phase -140 μA, 140 μs; anodic phase 180 μA, 100 μs and cathodic phase -180 μA, 100 μs; anodic phase 100 μA, 300 μs and cathodic phase -100 μA, 300 μs.

Asymmetric Waveforms

anodic phase 160 μA, 120 μs and cathodic phase -120 μA, 160 μs; anodic phase 180 μA, 100 μs and cathodic phase -100 μA, 180 μs; anodic phase 200 μA, 80 μs and cathodic phase -80 μA, 200 μs.

Stimulation frequencies ranged from 5 Hz to 130 Hz, depending on the specific treatment requirements. For depression treatment, a 130 Hz asymmetric waveform (anodic phase 180 μA, 100 μs and cathodic phase -100 μA, 180 μs) was delivered either as a single session or for 2 hours daily over the course of one week. Additionally, a 130 Hz symmetric waveform (anodic phase 200 μA, 50 μs and cathodic phase -200 μA, 50 μs) was used under the same protocol. To chronically activate the ACC and recapitulate depressive-like behaviors, a 20 Hz symmetric waveform (anodic phase 100 μA, 300 μs and cathodic phase -100 μA, 300 μs) was administered for 2 hours daily over a week.

DBS Parameter Optimization Experiments

To systematically determine effective stimulation parameters, we conducted a series of parameter screening experiments in awake, freely moving mice, ensuring that behavioral and physiological responses occurred under naturalistic conditions. Each mouse received a single trial of stimulation per parameter, consisting of ~25 minutes of continuous DBS. To prevent carryover effects, a washout period of at least 3 days was implemented between sessions. Due to occasional technical issues (e.g., fiber or electrode dislodgement), additional mice were introduced to ensure each stimulation condition was tested in a minimum of five animals.

The parameter testing sequence for CaMKII-*Cre* mice was structured as follows:

Inhibitory parameter screening (all at 130 Hz):

- Symmetric: 200 μA, 50 μs
- Symmetric: 140 μA, 140 μs
- Symmetric: 180 μA, 100 μs
- Asymmetric: 160 μA, 120 μs / -120 μA, 160 μs
- Asymmetric: 180 μA, 100 μs / -100 μA, 180 μs
- Asymmetric: 200 μA, 80 μs / -80 μA, 200 μs

Excitatory parameter screening:

Symmetric DBS (200 μA, 50 μs) tested at:

40 Hz → 15 Hz → 7 Hz → 5 Hz

Asymmetric DBS (180 μA, 100 μs / -100 μA, 180 μs) tested at:

80 Hz → 40 Hz → 15 Hz → 10 Hz

Additional chronic excitatory conditions included symmetric stimulation at 20 Hz and 130 Hz (100 μA, 300 μs / -100 μA, 300 μs). In addition, a new cohort of mice was tested with the same stimulation parameters at 15 Hz, as part of an extended analysis prompted by reviewer recommendations.

The parameter testing sequence for *Vgat-Cre* mice was structured as follows:

- Symmetric: 200 μA, 50 μs at 15 Hz → 40 Hz → 130 Hz
- Asymmetric: 180 μA, 100 μs / -100 μA, 180 μs at 130 Hz → 15 Hz
- Symmetric: 100 μA, 300 μs at 20 Hz

Please cite this article in press as: Yuan et al., Optimized deep brain stimulation for anterior cingulate cortex inhibition produces antidepressant-like effects in mice, Neuron (2025), https://doi.org/10.1016/j.neuron.2025.07.018

Immunohistochemistry

Mice were maintained in awake, freely moving conditions during DBS protocols to ensure physiological relevance. Immediately post-stimulation (15-minute time point selected based on preliminary optimization experiments and literature demonstrating robust pPDH induction kinetics), animals were deeply anesthetized with an overdose of pentobarbital (100 mg/kg, i.p.) and maintained in the same chamber until reaching a deep surgical plane of anesthesia. Mice then were transcardially perfused with cold phosphate-buffered saline (PBS), followed by cold paraformaldehyde (PFA, 4% wt/vol in PBS) within a 5-minute window to minimize anesthesia-induced artifacts. Control groups underwent identical anesthesia and perfusion procedures without DBS. Brains were removed and postfixed in 4% PFA for 4 hours at room temperature and then cryoprotected in 30% sucrose solution until tissues sank. Thin sections (35 μm) were prepared with a cryostat microtome (Leica CM1950). Samples were permeabilized in PBS with 0.3% Triton X-100 (PBST) and blocked in 3% BSA in PBST at room temperature for 1 hour. Sections were then incubated with primary antibodies [anti-NeuN, 1:1000, ab177487, Abcam, for 24 h; anti-PDH (phospho ser293), 1:500, 37115S, Cell Signaling Technology, for 48h] at 4°C. Samples were washed three times in PBST and were then incubated with fluorescent secondary antibodies (goat anti-rabbit Cy3, 1:500, 111-165-144, Jackson ImmunoResearch Labs) at room temperature for two hours. Samples were then washed three times in PBS.

pPDH imaging and quantification

Fluorescence imaging was performed using two distinct platforms to balance throughput and resolution. Widefield images (Figure 4A) were acquired using a VS120 Virtual Slide Microscope (Olympus) at 10× magnification. Acquisition settings were held constant across all samples to ensure comparability: light source intensity was set to 3V; Cy3 fluorescence was captured using a 605 nm filter with a 200 ms exposure; brain slice autofluorescence was imaged at 480 nm with a 50 ms exposure; and DAPI fluorescence was imaged at 455 nm with a 50 ms exposure.

Higher-resolution confocal images (Figure 4C) were obtained using a Leica TCS SP8 confocal microscope with a 20× objective. Laser power was maintained at 0.1% for the 488 nm laser and 0.5% for the 552 nm laser; detector gain was set at 750 (488 nm, PMT) and 70 (552 nm, HyD); and the pinhole diameter was fixed at 59.4 μm across all conditions. The apparent differences in background fluorescence between Figures 4A and 4C reflect differences inherent to the imaging modalities rather than variability in acquisition parameters within each dataset.

To quantify fluorescence intensity, whole-brain slice images were aligned to the Allen Mouse Brain Common Coordinate Framework (CCFv3) using ABBA (Aligning Big Brains and Atlases).[53,54] This included tilt and roll corrections, affine and spline-based in-plane registrations, and manual refinements. Aligned images and atlas annotations were imported into QuPath[55] for regional quantification. For each brain region, mean fluorescence intensities were calculated and normalized to corresponding anatomical regions in control mice (ACC-sham group) using the following equation: Normalized intensity = F_1 / F_0, where F_1 denotes fluorescence intensity in ACC-DBS mice and F_0 denotes the mean baseline intensity in ACC-sham controls. This region-matched normalization strategy accounted for inter-regional variability and standardized control values to unity across all analyzed brain regions.

QUANTIFICATION AND STATISTICAL ANALYSIS

We used MATLAB R2020a and GraphPad Prism 8.4.3 to perform statistical analysis. The methods of calculating the fluorescence changes in fiber photometry recording were similar to those described in previous studies.[10,47,52] Sample sizes (n) denote the number of mice used as reported in the figure legends. Data were reported as means ± SEM in all figures. The exact *P values* and the corresponding inferential statistical methods are stated in figure captions and legends. Detailed information on statistical tests is provided in Table S1.